2023-03-14

Large Deflection Analysis of General Beams in Contact-Aided Compliant Mechanisms Using Chained Pseudo-Rigid-Body Model

Mohui Jin
South China Agricultural University

Collin Ynchausti
Brigham Young University - Provo

Xianmin Zhang
South China University of Technology

Zhou Yang
South China Agricultural University

Benliang Zhu
South China University of Technology

See next page for additional authors

Original Publication Citation

"Jin, M., Yang, Z., Ynchausti, C., Zhu, B., Zhang, X, Howell, L.L., “Large Deflection Analysis of General Beams in Contact-Aided Compliant Mechanisms Using Chained Pseudo-Rigid-Body Model,” Journal of Mechanisms and Robotics, Vol. 12, paper no. 031005, 10 pages, doi:10.1115/1.4045425, 2020."

Large Deflection Analysis of General Beams in Contact-Aided Compliant Mechanisms Using Chained Pseudo-Rigid-Body Model

Mohui Jin
College of Engineering
South China Agricultural University
Guangzhou, China
Department of Mechanical Engineering
Brigham Young University
Provo, UT 84602, USA
Email: jinmohui@163.com

Collin Ynchausti
Department of Mechanical Engineering
Brigham Young University
Provo, UT 84602, USA

Xianmin Zhang
School of Mechanical and
Automotive Engineering
South China University of Technology
Guangzhou, China

The nonlinear analysis and design of contact-aided compliant mechanisms (CCMs) are challenging. This paper presents a nonlinear method for analyzing the deformation of general beams that contact rigid surfaces in CCMs. The large deflection of the general beam is modeled by using the chained pseudo-rigid-body model. A geometry constraint from the contact surface is developed to constrain the beam's deformed configuration. The contact analysis problem is formulated based on the principle of minimum potential energy and solved using an optimization algorithm. Besides, a novel technique based on the principle of work and energy is proposed to calculate the reaction force/moment of displacement-loaded cases. Several analysis examples of the compliant mechanisms with straight or curved beams are used to verify the proposed method. The results show that the proposed method and technique can evaluate the deformation of beam-based CCMs and the reaction force/moment with acceptable accuracy, respectively.

Zhou Yang
College of Engineering
South China Agricultural University
Guangzhou, China

*Corresponding author.

Email: yangzhou@scau.edu.cn

Benliang Zhu
School of Mechanical and
Automotive Engineering
South China University of Technology
Guangzhou, China

Larry L. Howell*
Department of Mechanical Engineering
Brigham Young University
Provo, UT 84602, USA
Email: lhowell@byu.edu

1 Introduction

Compliant mechanisms utilize the elastic deformation of their flexible components to transfer force and motion [1]. In general, their force and motion responses are smooth when the material model is continuous and/or buckling is not allowed [2]. Unlike the traditional compliant mechanisms, contact-aided compliant mechanisms (CCMs) [3] utilize mutual contact with external rigid bodies and/or self-contact with different parts of the mechanism itself to produce enhanced functionality, e.g., non-smooth path, motion and force-deflection characteristics.

Thanks to the above advantages, CCMs have been widely used. The concept of CCMs was firstly introduced by Mankame et al. [3] in a design of displacement-delimited contact-aided compliant grippers. They also used CCMs to solve the non-smooth path generation problems [4]. Howell et al. [5–8] proposed a class of compliant contact-aided revolute joints and applied it to spinal arthroplasty. Moon [9] designed a finger mechanism with a CCM. Mehta et al. [10] introduced CCMs into compliant cellular structures to achieve stress relief. CCMs were also used in the design of flapping wings [11–13], nonlinear stiffness actuators [14] and surgical devices [15]. Most of these CCMs utilize flexible beams that contact rigid surface, i.e., undergoing mutual contact. So this paper focuses on the nonlinear analysis of the beam-based CCMs with mutual contact.

The contact phenomenon in CCMs introduces strong boundary nonlinearities, which makes CCMs more difficult to be analyzed and designed than the traditional compliant mechanisms. In the field of computational contact mechanics, many different approaches have been developed. As the most popular approach, the finite element analysis (FEA) method that usually makes use of the Lagrange multipliers method and the penalty method [16] has been well established for the contact problems undergoing both small and large deformations [17]. Several kinds of penetration functions [18] that describe the normal distance between two bodies or beams have been defined for the contact constraint. Ref. [19] provides further details and references to the relevant literature. Since FEA has been well tested, the CCMs are usually analyzed and verified by using FEA to obtain the contact beams' deformation and the contact force/stress in the contact zone. Also, the contact FEA has been used in the topology optimization method proposed by Saxena and Kumar [20–22], which could optimally synthesize CCMs for path generation problems.

Although FEA is a powerful general tool for analyzing the CCMs with given shape and dimension, efficient and focused analysis models are still needed for CCMs for the following reasons: (i) In the design phase, the shape and dimension of the beams in CCMs usually need to be changed or optimized to fulfill the mechanisms' function, e.g., path generation or synthesis of load-deflection relationship. The number of analyses in the synthesis or optimization process could be very large, which requires the analysis method to be efficient. (ii) The computational contact mechanics behind FEA are general and applicable to a wide range of problems, but the more focused models, while not as general, can be better suited for being embed in shape or dimensional optimization programs. The analysis of CCMs is more about the contact's impact on the deformation and the required load of mechanisms rather than the contact force/stress in the contact zone. Consequently, a simple and easy-to-follow analysis method will be useful for the nonlinear contact analysis and design of CCMs.

During the past decades, a few analytical models have been developed for CCMs. For example, Cannon and Howell [5] modeled the required moment of a contact beam in a contact-aided revolute joint based on the relationship between beam's final curvature and moment. Moon [9] also used the Bernoulli-Euler beam theory to model the energy storage and required torque of a compliant contact-aided four-bar mechanism. Mehta et al. [10] proposed an analytical model for cellular structures by considering the contact effects. However, these models were all developed for particular CCMs.

In this paper, we try to propose a straightforward and general method for the contact analysis of CCMs based on one of the existing nonlinear analysis methods of compliant mechanisms, e.g., the pseudo-rigid-body model (PRBM) [23–26], chained PRBM (CPRBM) [27–29], beam constraint model (BCM) [30–33], elliptic integral solution (EIS) [34], etc. Currently, these methods focus on the problems without contact. The existing PRBMs in the literature are developed for particular beams,

i.e., straight and circular beams [35, 36]. So they are not applicable to the beams of general shape and can potentially be used for some particular cases of contact, e,g., beam with contact at its tip. The CPRBM proposed by Saggere and Kota [27] decomposes a general beam of various shape into $N \geq 3$ segments joined by N torsion springs. The whole deformed shape of the general beam can be obtained by this method, which lays a basis for this paper. Chen et al. [37] proposed an approach for the large deflection problems of spatial flexible rods using principal axes decomposition of compliance matrices. This approach also uses chained pseudo-rigid-body spatial mechanism to simulate the 3D deformation of flexible rods, which may be potentially extended to 3D contact problems. The chained BCM (CBCM) proposed by Chen et al. [33] is an accurate method for analyzing the general beams of various shape, and can be extended to 2D contact problems. Lastly, the EIS method is mainly used for large-deflection analysis of the beams with simple shape.

Compared with CBCM and the method proposed by Chen et al. [37], the modeling process of CPRBM is relatively simpler and more straightforward for the 2D problems. Moreover, the static equilibrium configuration of CPRBM is usually solved by using the principle of minimum potential energy, which makes it easy to embed the contact constraints into deformation analysis. Thus, this paper utilizes the concept of2 CPRBM to establish a simple and easy-to-follow contact analysis method for CCMs. A geometry-based contact constraint that describes the projection distance between the beam and the rigid surface is proposed to keep the joints of CPRBM out of the contact surface. The whole contact analysis problem is formulated based on the principle of minimum potential energy, i.e., finding the minimum potential energy of the compliant system under the geometry constraint from contact. By solving this constrained minimization problem, the static equilibrium position of CPRBM can be obtained. In the case of displacement-loaded CCMs, it is difficult to determine the reaction force at the input port of the mechanisms due to the complicated internal forces caused by contact. Hence, a novel technique based on the principle of work and energy is also proposed to calculate the reaction force of the displacement-loaded cases.

Compared with FEA, the proposed method offers following advantages: (i) It is simple and easy to implement the large-deflection analysis of the contact beams in general shapes. (ii) It facilitates the analysis of the CCMs with prestressed assembly. The contributions of this paper are as follows: A simple numerical method is proposed for the mutual contact analysis of CCMs. We analyze the introduced CPRBM based on the principle of minimum potential energy, and propose a geometry-based contact

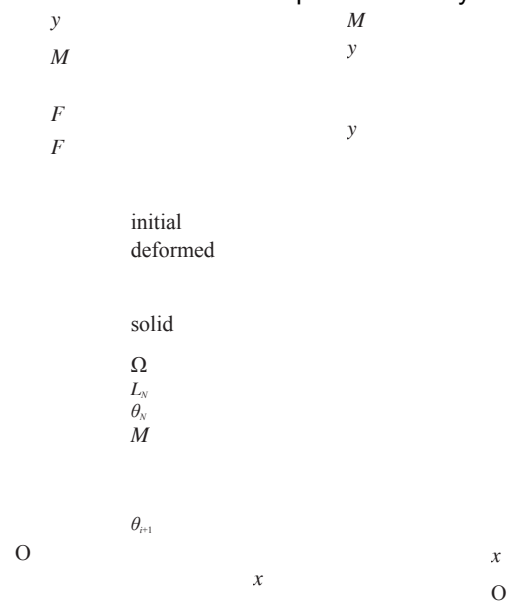

Fig. 1. A general beam that contacts a rigid object.

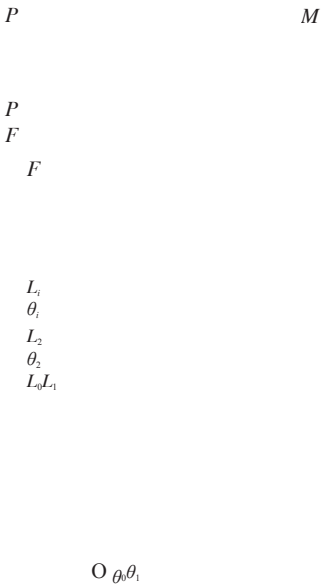

Fig. 2. A quarter circular beam and its CPRBM.

constraint formulation. In addition, a novel technique is proposed for calculating the reaction force of the displacement-loaded CCMs.

The rest of this paper is organized as follows. Section 2 describes the modeling of general beams, formulation of contact problems, and calculation of reaction forces. Section 3 gives several numerical examples to verify the proposed method. The discussions and conclusions are presented in Sections 4 and 5.

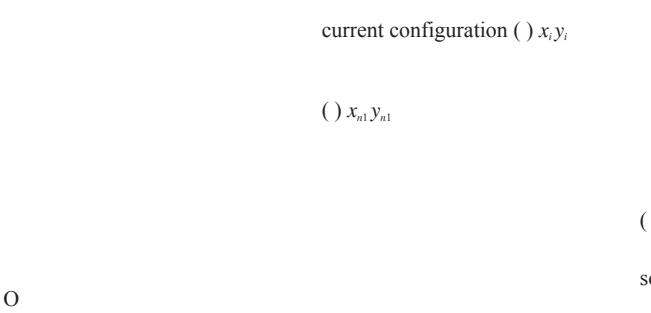

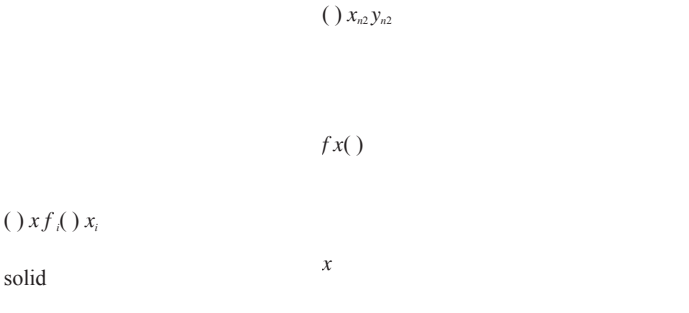

Fig. 3. Schematic for the contact constraints on the beam's current configuration. The joints within [$n1$, $n2$] will be constrained.

2 A general method for analyzing contact-aided beams A general beam with mutual contact is shown in Fig. 1. The beam will contact one or multiple rigid contact surfaces during its deformation process. In this paper, we focus on the large deformation of the contact-aided beams, and will not take the stress and friction between the beam and contact surface into account.

2.1 Modeling the large deflection of general beams As shown in Fig. 2, a general beam can be modeled as a series of small, straight, rigid elements connected end to end through linear torsional springs, i.e., CPRBM. The stiffness constant k_i of each torsional spring is approximately calculated as

$$k_i = \frac{EI}{L_i} i = 1, 2, \cdots, N \quad (1)$$

where EI is the bending stiffness of the beam element, L_i is the length of the rigid element, and N is the number of rigid elements. The first element L_0 is usually fixed to the ground. For a better analysis accuracy, our recommendation is that the length of the first element should be half of the other elements, i.e., $L_0 = 0.5L_i$, $i = 1, 2, \cdots, N$. When the number of elements N is large enough, the resulting CPRBM can equivalently describe the nonlinear load-deflection characteristics of a beam with general geometry shapes and load boundary conditions. Not only the beams' end position, but also their deformed shapes can be accurately described.

The static equilibrium problem of the CPRBM without contact is formulated based on the principle of minimum potential energy.

$$PE = \sum_{i=1}^{N} \frac{1}{2} k_i \delta^2_i - (P\Delta x + F\Delta y + M\Delta\theta_E) \quad (3)$$

where δ_i is the deformation of the ith torsional spring and is calculated as $\delta_i = (\theta_i - \theta_{i-1}) - (\theta'_i - \theta'_{i-1})$. θ_i and θ'_i are the final and initial tangent angles of the ith element, respectively.

$$x_i = \sum_{i-1} \sum_{j=0} L_j \cos(\theta_j), \quad y_i = \sum_{i-1} \sum_{j=0} L_j \sin(\theta_j) \quad (4)$$

Due to the contact between the solid surface and the deformed beam, the deformed configuration of the beam

$$\min PE$$
$$s.t. \quad \vec{Z}(\theta_1, \theta_2, \cdots, \theta_N) = 0 \quad (2)$$

By minimizing the potential energy function PE of this compliant system under the constraints of vector loop equation(s), $\vec{Z}(\theta_1, \theta_2, \cdots, \theta_N)$, we can obtain the static equilibrium position of the CPRBM, i.e., the deformed state of the beams. The potential energy function PE is the sum of torsional springs' potential energy and the conservative external forces' potential energy:

2.2 Formulation of mutual contact problems Without loss of generality, we discuss a general beam that contacts a rigid contact surface $f(x)$ shown in Fig. 3. The contact surface $f(x)$ is a continuous function. In the current configuration of the deformed beam, the position of each joint can be calculated as

should be outside of the rigid surface. Thus, a contact constraint $g(x_i, y_i)$ that describes the distance between each related joint and the contact surface $f(x)$ is introduced.

Figure 3 shows a current configuration of the deformed beam. For each related joint, whose position in this current configuration is (x_i, y_i), the coordinate of its projection point on the contact surface $f(x)$ in the direction of y-axis is $(x_i, f(x_i))$. Note that the position of the projection point changes with the deformation. According to the specific condition of the case in Fig. 3, the related joints should be above their corresponding projection points. Hence, the contact constraints for this case are formulated as

$$g(x_i, y_i) = f(x_i) - y_i \le 0,\ i \in [n1, n2] \quad (5)$$

where $[n1, n2]$ indicates region of the joints that potentially contact the rigid surface. The number of the contact constraints is equal to the number of the related joints. It should be pointed out that the direction of projection and the position relations between the related joints and corresponding projection points are determined according to the specific conditions of analysis problem.

Then, the contact constraints will be added into the static equilibrium problem in Eq. (2) to constrain the deformed configuration of the beam. The complete formulation of the mutual contact problems is

$$\min PE \quad s.t. \ \vec{Z}(\theta_1, \theta_2, \cdots, \theta_N) = 0 \ g(x_i, y_i) \le 0,\ i \in [n1, n2] \quad (6)$$

By solving the constrained minimum problem in Eq. (6), the deformed configuration of the beam can be obtained directly. However, the analysis of displacement-loaded cases cannot provide the information of the reaction force/moment F_{re}, and additional calculation is needed. Since the contact phenomenon may induce complicated internal forces between the flexible beam and rigid surface, it is hard to obtain F_{re} by solving the force balance equations in the deformed configuration.

Thus, we propose a new technique to calculate the reaction force/moment F_{re} based on the principle of work and energy. The nonlinear relationship between the input displacement d_{in} and F_{re} can be shown as Fig. 4. To calculate F_{re} for the input displacement d_{in}, two input displacements d_1 and d_2 are selected on the left side and right side of d_{in}, ρd_{in} displacement $d_1\ d_2\ d_{in}$ the current position of the related joint during

Fig. 4. Schematic for calculating the reaction force F_{re} of the displacement-loaded cases.

potential energy of torsional springs.

$$PE = \sum_{i=1}^{N} \frac{1}{2} k_i \delta^2_i \quad (7)$$

respectively.

$$d_1 = d_{in}(1-\rho),\ d_2 = d_{in}(1+\rho) \quad (8)$$

The step between d_1/d_2 and d_{in} is ρd_{in}, where ρ is the step ratio. When ρ is small enough, the load-displacement

The minimization problem in Eq. (6) is a complex minimization problem with multiple constraints, and can be solved by using different algorithms. The fmincon function in MATLAB is used here.

2.3 Calculation of the reaction force/moment at input port for displacement-loaded cases

In practical applications, many compliant mechanisms' input are displacements rather than forces. Then, the analysis problem is to find the deformation or reaction force/moment of the mechanism based on a known input displacement. For the displacement-loaded cases, the potential energy function PE only contains the elastic relationship within $[d_1, d_2]$ can be regarded as linear. If the input displacement increases from d_1 to d_2, the change of work ΔW can be calculated as

$$\Delta W = F_{re}(d_2 - d_1) = F_{re}(2\rho d_{in}) \quad (9)$$

The work increment ΔW is transformed into potential energy of springs, which is equal to the potential energy difference between d_1 and d_2:

$$\Delta W = \Delta PE = PE(d_2) - PE(d_1) \quad (10)$$

The potential energy $PE(d_1)$ and $PE(d_2)$ can be

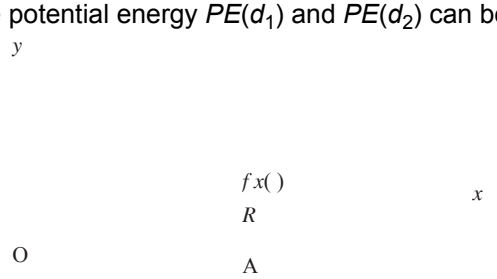

Fig. 5. A straight beam that contacts a rigid surface in the shape of semicircle.

positions caused by d_1 and d_2, respectively. Then, the reaction force/moment F_{re} is calculated as

$$F_{re} = \frac{PE(d_2) - PE(d_1)}{2\rho d_{in}} \quad (11)$$

The value of the step ratio ρ has an impact on the accuracy of the calculated reaction force F_{re}. When the value of ρ is too large, the load-displacement relationship within $[d_1, d_2]$ cannot be regarded as linear anymore, which will increase the modeling error of the work increment ΔW. Theoretically, the smaller the value of ρ is, the closer the calculated reaction force is to the accurate value. However, if the step ρd_{in} is too small, the denominator in Eq. (11) will be close to zero. This may induce the numerical instabilities that increase the error of the calculated reaction force. Thus, the step ratio ρ should take an appropriate value.

3 Analysis examples

3.1 Contact-aided straight beam

As shown in Fig. 5, a straight beam ($y = 0.5x$, $x \in [0, 0.1]$m) that contacts a circular surface is taken as the first example to verify the proposed method. There is a gap between the beam and the contact surface. The parameters of the beam are: $E = 2 \times 10^9$ Pa, thickness t = 1mm, and width w = 10mm. The rigid surface is in the shape of a semicircle defined by

$$f(x) = \sqrt{0.02^2 - (x-0.05)^2} \quad (12)$$

The number of rigid elements has an impact on the precision of the CPRBM. Thus, the impact of the elements' number N will be considered first. To model the straight beam using CPRBM, it is discretized uniformly by 10 and 20 elements, respectively. The joints within the range of $x_i \in [0.04, 0.06]$ are considered as the potential contact nodes and constrained by the contact constraints. A combined

obtained after determining the mechanism's equilibrium

4

Fig. 6. Comparison of the deformation of the contact-aided straight beam using CPRBM and nonlinear FEA. The CPRBM uses two different number of elements in the discretization, where N is the number of elements in the discretization.

One can see that contact phenomenon occurs between the deformed beam and the rigid surface. When the beam is discretized by 10 elements, the relative error of the beam's end displacement is 10.27%. Two factors contribute to this difference. One is that the element number is too small to obtain a CPRBM with high precision. Another one is caused by the intersection of the rigid link and the contact surface. Although joints 4 and 5 are on the side of the contact surface, the contact constraints on the two joints cannot prevent link 5 from intersecting with the contact surface when the link is too long. As the number of rigid elements increases, the errors caused by the two factors can be reduced. For the case of N = 20, the relative error of the beam's end displacement is below 0.5%. Not only the end position of the beam, but

load of F_{Ax} = 0.1N, F_{Ay} = −0.3N, and M_A = 0N · m is applied at the free end of the beam. The deformed configurations of the beam obtained by the proposed method are plotted in Fig. 6, and compared with the nonlinear FEA results from ANSYS, whose corresponding graphic result is shown in Fig. 7.

also its deformed shape obtained by the proposed method match well with the results of nonlinear FEA.

To evaluate the accuracy of the proposed method in large deflection problems, three load cases [F_{Ax}, F_{Ay}, M_A] are applied at the end of the straight beam. The three load cases are [0.1, −0.1, 0], [0.1, −0.3, 0], and [0.1, −0.5, 0], respectively. The straight beam is modeled by using 30 elements. The analysis results are shown in Fig. 8. The analysis results of CPRBM match well with the results from nonlinear FEA. Compared with the results from nonlinear FEA, the relative errors of the beam's end displacement for the three load cases are 0.58%, 0.33%, and 0.37%, respectively.

Fig. 7. Graphic result of ANSYS for the contact-aided straight beam with the load case of [0.1, −0.3, 0].

Fig. 8. Comparison of the results of CPRBM and nonlinear FEA for the contact-aided straight beam with different load cases.

3.2 Contact-aided curved beam

A compliant mechanism with two symmetrical curved beams and its modeling schematic are shown in Fig. 9. Due to symmetry, only the right half of the mechanism is analyzed here, whose equation is $x = 6.5y^2 + 0.002$, $y \in [-0.05, 0]$ m. The parameters of the beam are: $E = 2 \times 10^{11}$ Pa, thickness t = 1mm, and width w = 8mm. The rigid contact surface $f(x)$ is defined as

$$f(x) = -40x^2 - 0.037 \quad (13)$$

The curved beam is discretized uniformly along the y-axis by using 40 elements. The resulting joints within the range of $y \in [-0.05, -0.01)$ are constrained by the contact constraints. To show the displacement-loaded case, two different displacements (Δy = 10 and 20 mm) are chosen as the input for this mechanism, respectively. By solving the constrained static equilibrium problems, their deformed configurations can be obtained and shown in Fig. 10. Also, the deformation data obtained from the nonlinear FEA is plotted in the figure. The ANSYS graphic result for the case of Δy = 20 mm is shown in Fig. 11. The proposed CPRBM method can accurately describe the whole deformation of the curved beam and matches well with the FEA results. When the displacement of the beam's endpoint in the two displacement-loaded cases are considered, the relative

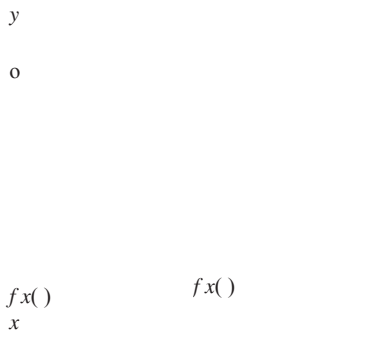

(a) (b)

Fig. 9. A compliant mechanism with (a) two symmetrical curved beams contacting a rigid surface $f(x)$ and (b) its modeling schematic.

Fig. 10. Comparison of the deformation obtained from CPRBM and nonlinear FEA.

errors between CPRBM and nonlinear FEA are 0.33% and 1.10%, respectively. For a better result, we can modify the discretization of CPRBM by discretizing the y-axis based on the recommendation shown in Section 2.1, i.e., $L_0 = 0.5L_i$, $i = 1, 2, \cdots, N$. Then, the two relative errors can be reduced to 0.05% and 0.14%. The rest analyses of this section are performed based on this improved discretization.

Before calculating the reaction force for the 6

Fig. 11. Graphic result of ANSYS for the input case of $\Delta y = 20$ mm.

displacement-loaded cases, the step ratio ρ's impact should be studied. With a given value of ρ and an input displacement Δy, a reaction force F_{re} can be obtained by using the proposed technique. To verify its accuracy, the obtained F_{re} is then regarded as the input for the force-loaded case to solve the corresponding displacement Δy_{force} at the force-loaded port. Here, the CPRBM for the displacement-loaded case is the same with the force-loaded case. Then, the force-displacement relationship at the input port should be the same theoretically for the two cases. In other words, Δy_{force} of the force-loaded case should be equal to Δy of the displacement-loaded case if the calculation of reaction force is accurate enough. By comparing Δy_{force} with Δy, we can verify the accuracy of the proposed technique. The accuracy here means that the proposed technique can solve the reaction force accurately for a given CPRBM. However, the error between the calculated F_{re} and the precise value still exists, which is caused by the accuracy of CPRBM.

Figure 12 shows the step ratio ρ's impact on the relative errors of Δy_{force} and Δy. Here, ρ varies from 0.02% to 2%, and Δy takes the three values of 10, 20, and 30 mm. The relative errors of the three input cases are all below 0.4% when ρ is less than 2%. The calculation of reaction force can be more accurate if ρ is less than 1%. The curve of $\Delta y = 10$ mm suffers from numerical instability in the range of $\rho \in [0.02\%, 0.2\%]$. Since the steps between d_1 and d_2 become quite small in this range, the corresponding relative errors increase, but are still in small values.

By setting the step ratio ρ to 0.5%, the relationship between the reaction force and input displacement can be obtained and is shown in Fig. 13. Six reaction forces obtained from the nonlinear FEA and the corresponding relative errors are also shown in this figure. Among those, the case of $\Delta y = 30$ mm has the maximum relative error, i.e., 3.5%. On the whole, the force-displacement relationship solved by the proposed technique matches with that of the nonlinear FEA.

Fig. 12. Impact of the step ratio ρ on the accuracy of reaction force calculations.

Fig. 13. Comparison of the force-displacement relationship of the contact-aided curved beam using the proposed technique and non linear FEA.

3.3 Deployable compliant mechanism with curved

beams

The third analysis example is a deployable compliant mechanism with two identical curved beams, i.e., curved beams AB and DC in Fig. 14. The rigid links AD and BC are considered as the fixed base and moving stage, respectively. Unlike traditional compliant parallelogram mechanisms, the main function of this mechanism is to deliver a vertical motion. This mechanism can be used as a cell of deployable mechanisms [38] that can expand linearly along direction of the *y*-axis. The upper surface of beams AB and DC will contact link BC, while the lower surface of the two beams will contact link AD. These contact pairs are shown in Fig. 14. The equation of curve AB is

$$x = (-7.4544s^5 + 18.636s^4 - 12.424s^3 + 20.0s) \times 10^{-3}$$

$$y = (3.4266s^7 - 11.993s^6 + 14.3916s^5 - 5.9964s^4 - 12.8706s^3 + 19.306s^2) \times 10^{-3}$$

$$s \in [0,\ 1] \tag{14}$$

The length of AD is equal to 30 mm. A vertical force F_y is added at point G, where $\overrightarrow{BG} = [5.62,\ 10]$ mm. The parameters of the curved beam are: $E = 2.3 \times 10^9$ Pa,

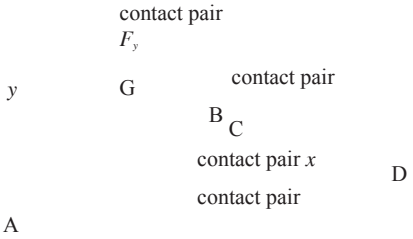

Fig. 14. A deployable compliant mechanism with two identical curved beams arranged in a parallelogram configuration.

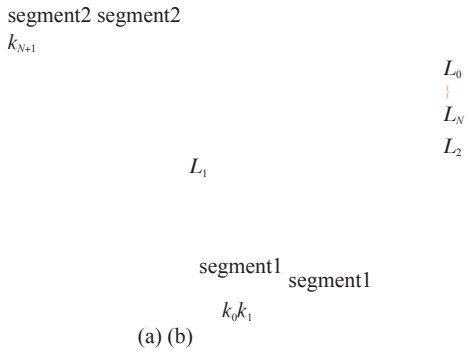

Fig. 15. Modeling schematic for the curved beams AB and DC.

thickness t = 1mm, and width w = 8mm. Each curved beam is discretized uniformly by using 60 elements. For this particular compliant mechanism, every point along the curved beam is potentially able to contact the rigid links. However, the first element of the general CPRBM shown in Fig. 2 is usually fixed, which makes the endpoint of the first element be unable to move and contact the rigid link. To simulate this particular kind of contact, the rotational DOF of the first element is freed here, as shown in Fig. 15. Then, the stiffness k_0 of the torsional spring at point A/D is calculated based on the length of the first element L_0. Similarly, we also free the rotational DOF of the last element by adding a torsional spring at its

Fig. 16. Comparison of the deformation of the deployable compliant

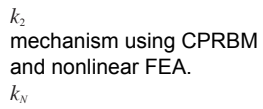

endpoint, which is located at point B/C. To calculate the stiffness of this torsional spring k_{N+1}, we divide the curved beam into two segments, i.e., segment1 and segment2. Here, segment1 is fixed to link AD, and segment2 is connected to link BC. For simplicity, we assume that the two segments are connected to each other at the middle of the last element. Then, the stiffness of the last two torsional springs, k_N and k_{N+1}, are determined based on half length of the last element, i.e., $L_N/2$. The stiffness of all the torsional springs are calculated as follows:

$$k_i = \frac{EI}{L_i} i = 0,\ 1,\ 2, \cdots,\ N-1$$

CPRBM match well with the results of FEA. The relative errors of the two curved beams' end displacements are $error_B$ = 2.50% and $error_C$ = 2.48% for the load case of F_y = −10 N. While the relative errors are $error_B$ = 0.12% and $error_C$ = 0.6% for the load case of F_y = −20 N.

Fig. 17. Graphic result of ANSYS for the deployable compliant mechanism with the load case of F_y = −20 N.

can be obtained. Figure 16 shows two deformations solved by using the CPRBM and the simulation results from the nonlinear FEA. The ANSYS graphic result for the case of F_y = −20 N is shown in Fig. 17. The curved beams do contact the rigid links and the results of

$$k_N = k_{N+1} = 2EI\,L_N \quad (15)$$

The potential energy function of this mechanism is constrained by the contact constraints and vector loop equations simultaneously. Through solving this minimum problem, the static equilibrium position of the mechanism

3.4 Partially compliant mechanism with one prestressed beam

As shown in Fig. 18(a), a hand gripper with one prestressed beam is taken as the last analysis example. This hand gripper is a partially compliant mechanism that consists of two rigid links and one initially straight beam. The straight beam will be prestressed after assembly. Due to symmetry, only the upper half of the gripper shown in Fig. 18(b) is considered for analysis. This mechanism is displacement-loaded by driving rigid link OA. When the link OA rotates clockwise, beam AB keeps contacting the

link OA. The length and initial tangent angle of link OA are 100 mm and 30°, respectively. The parameters of the straight beam are: E = 1.9 × 10^{11} Pa, length L_{beam} = 128 mm, thickness t = 0.254mm, and width w = 11mm.

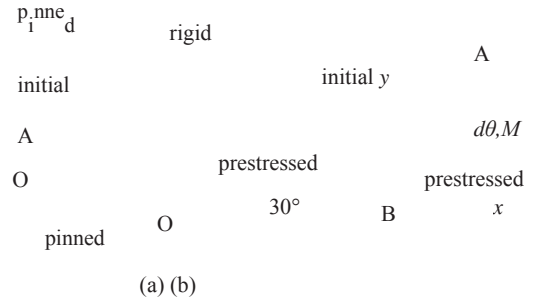

Fig. 18. A hand gripper with one prestressed beam: (a) prestressed assembly and (b) its modeling schematic.

shown in Fig. 18(b). The CPRBM discretization utilizes 40 elements, and is based on the recommendation shown in Section 2.1. Two thirds of the resulting joints are constrained by the contact constraints, i.e., $g(x_i, y_i) = y_i - f(x_i)$. In other words, the related joints should be under the rigid surface formed by the moving link OA. The endpoint B of beam AB is constrained in the freedoms of y and θ_z, so that it can slide along the x-axis. The endpoint A of beam AB should be in the position of link OA's endpoint. To show the displacement-loaded case, three different input displacements ($d\theta$ = 5°, 10°, 15°) are loaded at link OA, respectively. By solving the constrained static equilibrium problems, their deformed configurations can be obtained and are shown in Fig. 19. One can see that the contact part of the beam is increasing when link OA rotates clockwise. The contact effect also forces the curved beam to deform into the shape of link OA.

Fig. 19. Deformed configurations of the gripper for different input displacements.

The initial state of beam AB can be the one

For this displacement-loaded mechanism, it is hard to obtain its reaction moment by solving the force

balance equations. Whereas the proposed technique can solve the reaction moment without considering the internal forces between the contact pair. Like the study of reaction force in Section 3.2, the impact of step ratio ρ on the calculated reaction moment will be studied first. The value of ρ varies from 0.02% to 2%. The input displacement $d\theta$ takes the values of 5°, 10°, and 15°, respectively. With the given values of ρ and $d\theta$, the reaction moments can be obtained. Then, the solved reaction moments are used to calculate the angular displacements of link OA $d\theta_{force}$ for the force-loaded cases. The relative errors between $d\theta_{force}$ and $d\theta$ are shown in Fig. 20. The relative errors for the three input displacements are all below 0.15% when ρ is less than 2%.

Fig. 20. Impact of the step ratio ρ on the accuracy of reaction moment calculations.

Finally, a prototype experiment of this mechanism is carried out to verify the analysis accuracy of the proposed method. The setup for this experiment is shown in Fig. 21. To achieve large deformation, the straight beam is made of a spring steel strip. The two rigid links are manufactured by using plastic 3D printing. The upper rigid link is driven by a horizontal shaft, on which a torque sensor and a displacement sensor are mounted. With this system, the driving moments and angular displacements of the prototype can be measured. The experimental and nonlinear FEA results of the force-displacement relationship are plotted in Fig. 22. This figure also shows the force-displacement relationship obtained by the proposed technique, where the step ratio ρ is set to 0.5%. After the prestressed assembly, i.e., $d\theta = 0$, the static equilibrium configuration of the straight beam is shown in the right part of Fig. 21. The corresponding reaction moment of this configuration is 0.167 N·m. As the rigid link rotates clockwise, the deformation and reaction moment increase nonlinearly. When $d\theta = 14°$, the reaction moment increases to 0.67 N·m. Note that $d\theta$ is the change of the driving shaft's tangent angle, which is half of the angle marked in Fig. 21. By comparing the results from the proposed technique, experiment and nonlinear FEA, the result of the proposed technique match well with that of experiment and nonlinear FEA. The experimental force-displacement curve is close to the simulated one. The relative errors between the proposed technique and the nonlinear FEA are below 0.5%. Thus, our method can accurately evaluate the reaction moment of this mechanism. When $d\theta$ is larger than 13°, e.g., the configuration shown in the lower left corner of Fig. 21, the difference between the experimental and simulated results increases. This is caused by the plastic deformation at the middle of the straight beam.

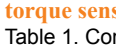

Fig. 21. Experiment setup for the partially compliant mechanism with one prestressed beam.

Table 1. Comparison of the computation time of the proposed method and 2D FEA

Methods	1st case	2nd case	3rd case	4th case
CPRBM	0.0905 s	0.5534 s	2.1306 s	0.4952 s
2D FEA	15 s	15 s	7 s	30 s

springs. One advantage of the proposed method is that it facilitates the analysis of the CCMs with rigid joints or prestressed assembly, e.g., the example in Section 3.4. Because the modeling process of the CCMs with prestressed assembly is as simple as the normal one. On the contrary, it

Fig. 22. Comparison of the force-displacement relationships ob tained by the proposed technique, experiment, and nonlinear FEA.

4 Discussions

All the numerical examples in this paper were carried out on a computer with Intel Core i5-4570 (3.20 GHz) CPU, 8.00GB RAM, and MATLAB R2018b. The computation time of CPRBM and 2D FEA for the four analysis examples are listed in Table 1. The result indicates that the proposed method spends less time than 2D FEA in the analysis of CCMs. The CPRBM's computation time for the third case is 2.1306 s, because its number of variables is 120. The FEA's computation time for this case is 7 s, which is much less than other FEA cases. The reason for this is that the two curved beams in Fig. 14 are in special shape of Euler spiral. With the special characteristic of linear curvature variation, the two Euler spiral flexures will deform into flat shape mainly due to their tip loads. The contact has less contribution to the deformation, which saves the computation time of FEA.

The proposed method currently focuses on analyzing the large deformation of contact-aided beams, including the output motion/trajectory, deformed shape, and load-deflection relationship of CCMs. The obtained deformation of the beam can be a basis for the analysis of stress. We can evaluate the maximum stress of each straight beam element based on the angular deformation of torsional

is not easy for ANSYS to analyze the CCMs with prestressed assembly. One feasible method is to use multiple load steps and one auxiliary force. The key modeling process is as follows: (1) Model the mechanism without prestressed assembly and let beam AB be in the vertical direction. The endpoint A of the straight beam is pinned to link OA, while the endpoint B is freed. (2) In the first load step, the endpoint B's rotational freedom is fixed, and its position is constrained to the x-axis. Meanwhile, $d\theta$ is set to zero. A horizontal force is acted on the endpoint B to avoid buckling. (3) In the second load step, set the auxiliary force to zero and keep $d\theta = 0$. The beam will deform to the static equilibrium configuration. (4) In the third load step, add the rotational displacement on link OA. The whole process in ANSYS requires careful modeling, or it will be easy to suffer convergency problems.

The analysis examples show that the CPRBM of straight beams can achieve a better accuracy than that of initially curved beams. For example, the result of the fourth analysis case has a better accuracy than that of the second analysis case. The accuracy of the deformation analysis and the reaction force/moment calculation can be improved by using a more precise CPRBM. The current CPRBM regards each flexible segment of the general beam as a straight beam and replaces it by a 1R PRBM. The axial direction of each straight beam is considered as rigid, which may increase the modeling error of the cases with large axial deformation. For those cases with large axial deformation, the CPRBM can be a compliant system with flexible rod elements and torsional springs.

One limitation of the proposed method is that the contact surface function $f(x)$ should be continuous and differentiable within the motion ranges of the related joints in contact constraints. Because the fmincon function in MATLAB is a gradient-based method that requires the objective and constraint functions to be continuous and differentiable.

5 Conclusions

In this paper, a numerical method is proposed for the large-deflection analysis of CCMs undergoing mutual contact. The CPRBM and contact constraints are used to model and constrain the large deflection of general beams,

respectively. The static equilibrium position of the contacted beams are obtained by solving the minimum potential energy problem with the contact constraints. The analysis results of the proposed method match well with the nonlinear FEA results, which proves the feasibility of this method in the contact analysis of general beams and partial compliant mechanisms. Besides, this paper proposed a novel technique to calculate the reaction force of the displacement-loaded contact problems based on the principle of work and energy. The impact of the step ratio ρ on the accuracy of reaction force calculation is also studied.

The proposed method is simple and straightforward, and can be an alternative to FEA in the analysis of CCMs. Its computational efficiency can be an advantage when a series of analysis is needed, especially in the conceptual design stage of CCMs. In addition, the proposed analysis method and the technique for reaction force/moment calculation can also be applied to the problems without contact. The analysis of the self-contact between two flexible beams will be included in our future work.

Achnowledgements

The authors gratefully acknowledge the financial support from the Young Innovative Talents Program of Universities in Guangdong (Grant Nos. 2018KQNCX018 and 2018KQNCX021), the CSC Scholarship, and the National Natural Science Foundation of China (Grant No. 51675189).

References

[1] Howell, L. L., 2001. *Compliant Mechanisms*. John Wiley & Sons, Inc, New York.

[2] Mankame, N. D., and Ananthasuresh, G., 2004. “Topology optimization for synthesis of contact-aided compliant mechanisms using regularized contact modeling”. *Computers & structures,* 82(15-16), pp. 1267– 1290.

[3] Mankame, N. D., and Ananthasuresh, G., 2002. “Con tact aided compliant mechanisms: concept and prelimi naries”. In ASME 2002 International Design Engineering Technical Conferences and Computers and Information in Engineering Conference, American Society of Mechanical Engineers, pp. 109–121.

[4] Mankame, N. D., and Ananthasuresh, G., 2004. “A novel compliant mechanism for converting reciprocat ing translation into enclosing curved paths”. *Journal of Mechanical Design,* 126(4), pp. 667–672.

[5] Cannon, J. R., and Howell, L. L., 2005. “A compliant contact-aided revolute joint”. *Mechanism and Machine Theory,* 40(11), pp. 1273–1293.

[6] Halverson, P. A., Howell, L. L., and Bowden, A. E., 2008. “A flexure-based bi-axial contact-aided compli ant mechanism for spinal arthroplasty”. In ASME 2008 International Design Engineering Technical Conferences and Computers and Information in Engineering Conference, American Society of Mechanical Engineers, pp. 405–416.

[7] Montierth, J. R., Todd, R. H., and Howell, L. L., 2011. “Analysis of elliptical rolling contact joints in compression”. *Journal of Mechanical Design,* 133(3), p. 031001.

[8] Nelson, T. G., Lang, R. J., Magleby, S. P., and Howell, L. L., 2016. “Curved-folding-inspired deployable compliant rolling-contact element (D-CORE)”. *Mechanism and Machine Theory,* 96, pp. 225–238.

[9] Moon, Y.-M., 2007. “Bio-mimetic design of finger mechanism with contact aided compliant mechanism”. *Mechanism and Machine Theory,* 42(5), pp. 600–611.

[10] Mehta, V., Frecker, M., and Lesieutre, G. A., 2009. “Stress relief in contact-aided compliant cellular mechanisms”. *Journal of Mechanical Design,* 131(9), p. 091009.

[11] Tummala, Y., Wissa, A., Frecker, M., and Hubbard, J. E., 2014. “Design and optimization of a contact aided compliant mechanism for passive bending”. *Journal of Mechanisms and Robotics,* 6(3), p. 031013.

[12] Calogero, J., Frecker, M., Hasnain, Z., and Hubbard Jr, J. E., 2016. “A dynamic spar numerical model for passive shape change”. *Smart Materials and Structures,* 25(10), p. 104006.

[13] Calogero, J., Frecker, M., Hasnain, Z., and Hubbard, J. E., 2018. “Tuning of a rigid-body dynamics model of a flapping wing structure with compliant joints”. *Journal of Mechanisms and Robotics,* 10(1), p. 011007.

[14] Song, Z., Lan, S., and Dai, J. S., 2019. “A new mechanical design method of compliant actuators with non-linear stiffness with predefined deflection-torque profiles”. *Mechanism and Machine Theory,* 133, p p. 164–178.

[15] Eastwood, K. W., Francis, P., Azimian, H., Swarup, A., Looi, T., Drake, J. M., and Naguib, H. E., 2018. “De sign of a contact-aided compliant notched-tube joint for surgical manipulation in confined workspaces”. *Journal of Mechanisms and Robotics,* 10(1), p. 015001.

[16] Wriggers, P., Rust, W., and Reddy, B., 2016. “A virtual element method for contact”. *Computational Mechanics,* 58(6), pp. 1039–1050.

[17] Wriggers, P., and Zavarise, G., 1997. “On contac t between three-dimensional beams undergoing large deflections”. *Communications in numerical methods in engineering,* 13(6), pp. 429–438.

[18] Litewka, P., 2010. *Finite element analysis of beam-to beam contact*. Springer Science & Business Media. [19] Wriggers, P., 2002. *Computational contact mechanics*. John Wiley & Sons, Chichester.

[20] Saxena, A., 2013. “A contact-aided compliant displacement-delimited gripper manipulator”. *Journal of Mechanisms and Robotics,* 5(4), p. 041005.

[21] Kumar, P., Sauer, R. A., and Saxena, A., 2016. “Synthesis of c0 path-generating contact-aided compliant mechanisms using the material mask overlay method”. *Journal of Mechanical Design,* 138(6), p. 062301.

[22] Kumar, P., Saxena, A., and Sauer, R. A., 2019. 11 “Computational synthesis of large deformation compli ant mechanisms undergoing self and mutual contact”. *Journal of Mechanical Design,* 141(1), p. 012302.

[23] Howell, L. L., and Midha, A., 1995. “Parametric deflection approximations for end-loaded, large deflection beams in compliant mechanisms”. *ASME J. Mech. Des.,* 117(1), pp. 156–165.

[24] Venkiteswaran, V. K., and Su, H.-J., 2016. “A three spring pseudorigid-body model for soft

joints with significant elongation effects". *Journal of Mechanisms and Robotics,* 8(6), p. 061001.
[25] Yu, Y.-Q., and Zhu, S.-K., 2017. "5r pseudo-rigid-body model for inflection beams in compliant mechanisms". *Mechanism and Machine Theory,* 116, pp. 501–512.
[26] Zhu, S.-K., and Yu, Y.-Q., 2017. "Pseudo-rigid-body model for the flexural beam with an inflection point in compliant mechanisms". *Journal of Mechanisms and Robotics,* 9(3), p. 031005.
[27] Saggere, L., and Kota, S., 2001. "Synthesis of planar, compliant four-bar mechanisms for compliant-segment motion generation". *Journal of Mechanical Design,* 123(4), pp. 535–541.
[28] Pauly, J., and Midha, A., 2006. "Pseudo-rigid body model chain algorithm, part 1: introduction and concept development". In ASME 2006 International Design Engineering Technical Conferences and Computers and Information in Engineering Conference, American Society of Mechanical Engineers, pp. 173– 181.
[29] Pauly, J., and Midha, A., 2006. "Pseudo-rigid-body model chain algorithm, part 2: equivalent represen tations for combined load boundary conditions". In ASME 2006 International Design Engineering Technical Conferences and Computers and Information in Engineering Conference, American Society of Mechanical Engineers, pp. 183–190.
[30] Awtar, S., and Sen, S., 2010. "A generalized constraint model for two-dimensional beam flexures: nonlinear load-displacement formulation". *Journal of Mechanical Design,* 132(8), p. 081008.
[31] Ma, F., and Chen, G., 2016. "Modeling large planar deflections of flexible beams in compliant mechanisms using chained beam-constraint-model". *Journal of Mechanisms and Robotics,* 8(2), p. 021018.
[32] Ma, F., and Chen, G., 2017. "Bi-bcm: A closed form solution for fixed-guided beams in compliant mechanisms". *Journal of Mechanisms and Robotics,* 9(1), p. 014501.
[33] Chen, G., Ma, F., Hao, G., and Zhu, W., 2019. "Modeling large deflections of initially curved beams in compliant mechanisms using chained beam constraint model". *Journal of Mechanisms and Robotics,* 11(1), p. 011002.
[34] Zhang, A., and Chen, G., 2013. "A comprehensive elliptic integral solution to the large deflection problems of thin beams in compliant mechanisms". *Journal of Mechanisms and Robotics,* 5(2), p. 021006.
[35] Venkiteswaran, V. K., and Su, H.-J., 2016. "Pseudo rigid-body models for circular beams under combined tip loads". *Mechanism and Machine Theory,* 106, pp. 80–93.
[36] Venkiteswaran, V. K., and Su, H.-J., 2018. "A versatile 3R pseudo-rigid-body model for initially curved and straight compliant beams of uniform cross section". *Journal of Mechanical Design,* 140(9), p. 092305.
[37] Chen, G., Zhang, Z., and Wang, H., 2018. "A general approach to the large deflection problems of spatial flexible rods using principal axes decomposition of compliance matrices". *Journal of Mechanisms and Robotics,* 10(3), p. 031012.
[38] Ynchausti, C., Magleby, S. P., Bowden, A. E., and Howell, L. L., 2019. "Deployable euler spiral connec tors (DESCs)". In ASME 2019 International Design Engineering Technical Conferences and Computers and Information in Engineering Conference, American Society of Mechanical Engineers.